

# Quantum suppression of cold reactions far from the quantum regime

Or Katz,<sup>1,2,\*</sup> Meirav Pinkas,<sup>1</sup> Nitzan Akerman,<sup>1</sup> and Roei Ozeri<sup>1</sup>

<sup>1</sup>*Department of Physics of Complex Systems, Weizmann Institute of Science, Rehovot 7610001, Israel*

<sup>2</sup>*Present address: Department of Electrical and Computer Engineering,  
Duke University, Durham, North Carolina 27708, USA*

(Dated: August 17, 2022)

Reactions between pairs of atoms are ubiquitous processes in chemistry and physics. Quantum scattering effects on reactions are only observed at extremely ultracold temperatures, close to the  $s$ -wave regime, with a small number of partial waves involved. At higher temperatures, the different phases associated with the centrifugal barriers of different partial waves average-out quantum interference to yield semi-classical reaction rates. Here we use quantum-logic to experimentally study resonant charge-exchange reactions between single cold pairs of neutral  $^{87}\text{Rb}$  atoms and optically-inaccessible  $^{87}\text{Rb}^+$  ions far above the  $s$ -wave regime. We find that the measured charge-exchange rate is greatly suppressed with respect to the semi-classical prediction. Our results indicate for the first time that quantum interference persists and effects reaction rates at very high temperatures, at least three orders of magnitude higher than the ultracold  $s$ -wave regime.

## I. INTRODUCTION

Studies of chemical reactions between pairs of atoms are of great applicable and fundamental importance in chemical and physical sciences. At ultra-cold temperatures, the wave-like nature of the reactants plays a major role in determining the likelihood and pathways of a reaction. Quantum-mechanical effects such as shape resonances [1] or Feshbach resonances [2, 3] can enhance or suppress the reaction rate, provide control over the interaction strength, and allow for precise experimental calibration of the molecular potentials that are otherwise hard to compute. Beyond their fundamental importance, quantum scattering resonances practically provide control over interactions in quantum simulators [4–6] or used to push the limits of precision quantum sensors [7, 8]

Quantum scattering effects between pairs of atoms however are mostly limited to ultra-cold temperatures, where only few partial waves are involved [9–15]. The matter-wave length scale for entering the  $s$ -wave regime in atomic collisions of neutral atoms is typically a few nm which for typical atomic masses translates to an energy scale of 100's  $\mu\text{K}$  for entering the quantum scattering regime. This limitation originates from the fact that the range of the Van der Waals interaction; by which inelastic or reactive scattering processes are governed; is on par with that of centrifugal forces which are partial wave dependent. The phases acquired when colliding on different partial waves are largely different and the effect of multiple partial wave interference on the reaction cross-sections, averages to yield a semi-classical result.

Collisions between a neutral atom and a charged ion on the other hand, are governed by the long-range polarization potential which requires a matter-wave length

scale of 100's nm in order to enter the  $s$ -wave regime, and therefore a sub- $\mu\text{K}$  temperature for most atom-ion pairs [13, 14, 16–19]. The other side of the long-range interaction is that here centrifugal forces act at nuclei separations in which inelastic or reactive processes do not occur at all, while at molecular distances in which chemistry does occur centrifugal forces are negligible. It has been thus predicted that resonant inelastic and reactive processes, such as the exchange of electronic spins or the exchange of charge between identical nuclei [20, 21] could feature quantum signatures that persist at much higher temperatures, even up to 100's mK. This mechanism, coined as the partial-wave phase-locking mechanism, originates from the fact that the scattering phases of many partial waves are the same as that of the  $s$ -wave, leading to  $s$ -wave behaviour and quantum interference phenomenon far outside the  $s$ -wave regime.

Hybrid atom-ion platforms provide great experimental control with resolution of single collision events between pairs of atoms [16, 22–43], and are therefore good candidates to study the matter-wave phase-locking mechanism and unveil quantum signatures far from the quantum regime. Most studies of resonant processes between atoms and ions to date were carried out either at very hot temperatures [44–46], or at conditions for which the absolute collision rate was subject to uncertainty, hence quantum effects far from the  $s$ -wave regime have yet to be reported in any ultracold system. It should be noted that the matter-wave phase locking mechanism is intrinsic to longer range interactions and not specific to atom-ion systems.

Here we study resonant charge-exchange reactions between ultra-cold  $^{87}\text{Rb}$  atoms and a cold  $^{87}\text{Rb}^+$  ion. While  $^{87}\text{Rb}^+$  has no optical transitions that allow for its direct cooling or detection, we measure its reaction by applying a recently developed quantum-logic technique using an auxiliary  $^{88}\text{Sr}^+$  logic ion [47]. We further develop a method to determine the Langevin-

---

\* Corresponding author: or.katz@duke.edu

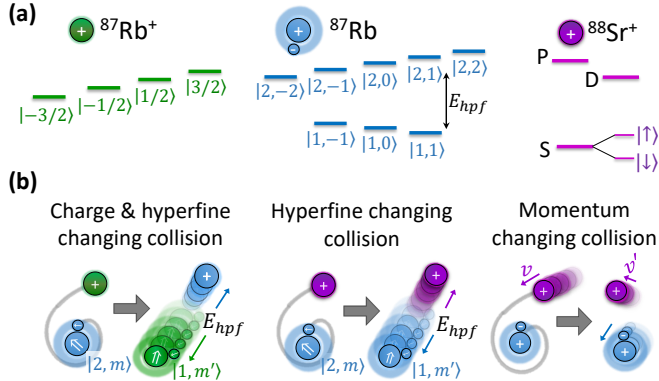


Figure 1. **Atom-ion cold collisional processes and spin structure.** (a) nuclear spin structure of  $^{87}\text{Rb}^+$  (left), hyperfine structure of  $^{87}\text{Rb}$  in its electronic ground-state (middle) and ground and first excited state manifolds for spin  $1/2$   $^{88}\text{Sr}^+$  (right). (b) Resonant charge-exchange reactions between  $^{87}\text{Rb}$ - $^{87}\text{Rb}^+$  (left) and spin-exchange collisions between  $^{87}\text{Rb}$ - $^{88}\text{Sr}^+$  (middle) can both change the hyperfine state of the neutral atom and convert the internal hyperfine energy  $E_{\text{hpf}}$  into kinetic motion of the bodies. Elastic collisions of an ion with a neutral atom (right) conserve the total momentum of the pair but change the trapped ion's momentum.

collision probability the ion experiences via measurement of momentum-changing collisions, which in turn enables estimation of the reaction probability in terms of Langevin collision rate. The observed reaction rate is suppressed by 12-fold with respect to the semi-classical value, even though the collision energy is more than three orders of magnitude higher than the  $s$ -wave regime. Our results provide a unique view on properties of the quantum  $s$ -wave regime at temperatures that are more than three orders of magnitude away, with techniques that can be readily applied to study other processes, species and systems.

## II. ATOM-ION COLLISIONS

The interaction between a neutral atom and a singly-ionized ion at an inter-nuclear distance  $R$  is composed of two different terms which dominate at complementary regimes. At long distances, the electric field of the ion's charge induces an electric dipole moment of the neutral atom and results with an attractive polarization potential that scales as  $-1/R^4$ , and depends only on the neutral atom polarizability [16]. If the initial angular momentum is not too large, in a semi-classical picture this attractive potential leads to inward spiraling of the pair, coined as Langevin collisions, until a close contact is made [17, 48].

At short inter-nuclear distances, non-universal chemical forces dominate the interaction. These forces

originate from significant overlap of the atomic wave-functions which can efficiently change the momentum, internal state or chemical composition of the colliding bodies [16]. In cold atom-ion systems, scattering events that involve a considerable change in the external or internal properties of the complex are typically correlated with Langevin collision events. Therefore, the rate of such processes typically takes a fraction of the Langevin rate.

### A. Resonant charge-exchange

Charge-exchange collisions are reactions in which the nuclei of the ion and neutral atoms are exchanged. This exchange originates from a differential scattering phase shift between the *gerade* and *ungerade* components of the wave-function of the colliding nuclei, the total nuclear spin of which is odd and even respectively [49, 50]. For hetero-nuclear species, the charge exchange rate is attenuated by the ionization energy mismatch between the two species [22]. For homo-nuclear species on the other hand, the aforementioned energy mismatch vanishes and the process is considered resonant and is expected to be very efficient. At cold temperatures which are yet far from the  $s$ -wave energy (above  $E_s = 79 k_B \times \text{nK}$  for  $^{87}\text{Rb}^+ - ^{87}\text{Rb}$  [17]), when many partial waves ( $L \gg 1$ ) contribute to the exchange, the

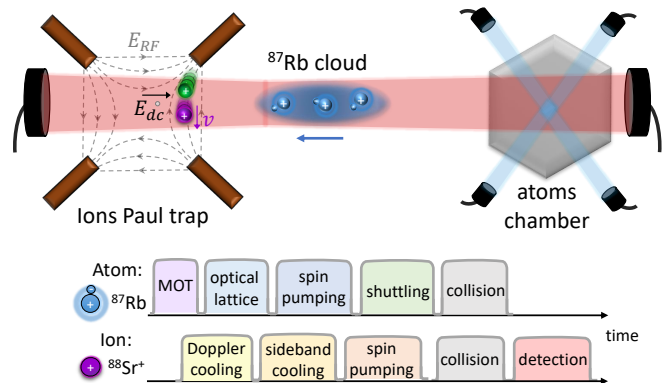


Figure 2. **Experimental Apparatus and Protocol** We trap neutral  $^{87}\text{Rb}$  atoms in the right chamber and short crystals of  $^{87}\text{Rb}^+$  and  $^{88}\text{Sr}^+$  ions in the left chamber. The ion crystal is laser-cooled near the motional ground-state. We load an atomic cloud into an off-resonant optical lattice dipole trap and shuttle it through the ion's Paul trap to allow for a collision. In measurement of hyperfine changing collisions excess micromotion is compensated but in measurement of momentum-changing collisions a time-independent electric field  $E_{\text{dc}}$  pushes the ions from the RF null of the trap, giving them excess micro-motion energy along the RF field lines.

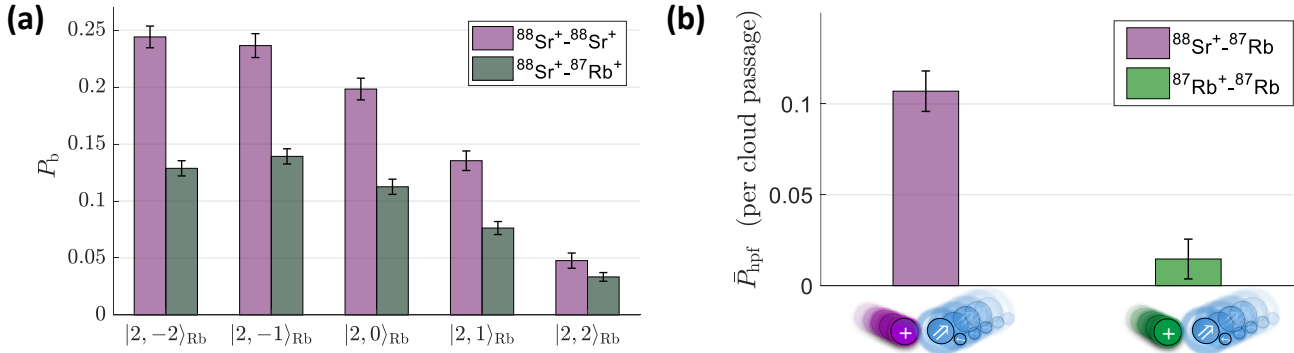


Figure 3. **Hyperfine changing collision probability and Logic detection**. (a) Raw measured probability of hyperfine changing collision by at least one ion in a  $^{87}\text{Rb}^+ - ^{88}\text{Sr}^+$  crystal (dark green) or  $^{88}\text{Sr}^+ - ^{88}\text{Sr}^+$  crystal (purple). (b) We use the raw data to distinguish between hyperfine changing collisions of  $^{87}\text{Rb}$  that originate from a collision with the  $^{88}\text{Sr}^+$  ion (purple) or from collision with the  $^{87}\text{Rb}^+$  ion (green) using the quantum logic technique (see text and Methods). The probability in (b) is given per ion per passage of the cloud through the trap. Bars represent  $1\sigma$  binomial uncertainties.

cross section is given approximately by [20]

$$\sigma_{\text{ex}} \approx \xi \left( \frac{1}{L} \sum_{l=0}^L \sin^2(\delta_g^{(l)} - \delta_u^{(l)}) \right) \sigma_L. \quad (1)$$

Here  $\sigma_L$  is the Langevin cross-section,  $\delta_g^{(l)}$  and  $\delta_u^{(l)}$  are the *gerade* and *ungerade* scattering phase shifts of the  $l$  partial wave, and the factor  $0 \leq \xi \leq 1$  hosts the spin dependence of the colliding bodies, depending on the initial spin states and the output channels being considered. Under the classical rapid-phase approximation [21, 51], the average contribution of each partial wave in Eq. (1) is  $1/2$ , yielding the classical cross-section  $\sigma_{\text{ex}} = \xi \sigma_L / 2$  [20, 22, 46, 50]. If the colliding atoms have no nuclear spin, or if the transition to all final channels is allowed, then  $\xi = 1$  (See Methods).

While resonant charge-exchange collisions do not change the specie of the ion, they can be observed via change of external or internal degrees of freedom. Resonant charge-exchange collisions are typically observed at high collision energies (above  $100 k_B \times \text{K}$  for  $^{87}\text{Rb}^+ - ^{87}\text{Rb}$ ), via efficient exchange of momentum [44–46] or spin [52, 53]. The former can enhance the cooling rate between a hot ion and a cold atomic bath by tunneling that occurs during elastic (glancing) collisions [46] and the latter allows for efficient orientation of the nuclear spin of the ions. At colder energies however, identification of such charge-exchange processes by their induced momentum change is challenging [54].

We probe charge-exchange collisions between cold  $^{87}\text{Rb}^+$  and  $^{87}\text{Rb}$  pairs via their induced change of the spin state.  $^{87}\text{Rb}^+$  has a nuclear spin  $3/2$ , and four spin levels that are very weakly split in energy owing to the weak nuclear gyro-magnetic ratio [55]. Neutral  $^{87}\text{Rb}$  has an additional electron spin  $1/2$  which is strongly coupled to the nuclear spin via the hyperfine interaction ( $E_{\text{hpf}} = 328 k_B \times \text{mK}$ ). This interaction renders

the total atomic spin of the rubidium atoms and their projection along the magnetic field axis to be good quantum numbers, denoted by  $F, M$ . The level structure of these atoms in the electronic ground state is shown in Fig. 1.

During a charge-exchange collision, the nuclear spin of the Rb ion is abruptly exchanged with that of the neutral Rb, which could lead to projection of the neutral Rb from the upper hyperfine manifold into the lower one. This transition is accompanied by release of the internal hyperfine energy, and its conversion into kinetic energy of the colliding bodies as shown in Fig. 1. We estimate the probability for such hyperfine transition during a cold charge-exchange collision using the semiclassical Degenerate Internal State Approximation and find that  $\xi = 3/8$  (see Methods). The overall classical cross-section for hyperfine change via charge exchange in this configuration is thus  $\sigma_{\text{ex}} = 3\sigma_L/16$ .

Experimental determination of the absolute scale of the charge-exchange rate therefore requires calibration of the probability of a Langevin collision in an experiment.

## B. Langevin collisions

Standard techniques estimate the Langevin probability via characterization of the atomic number-density  $n(r)$  of the neutral cloud at position  $r$  as well as estimation of the effective interaction time  $\tau$  [14, 16, 21, 22, 31]. Assuming an energy-independent Langevin rate coefficient in free space allows for experimental estimation of the Langevin rate  $\kappa_L$ . However, such technique is typically prone to systematic uncertainties primarily in the atomic number-density and in the Langevin rate coefficient, whose value depends on the trap parameters [18].

We consider a different technique to estimate

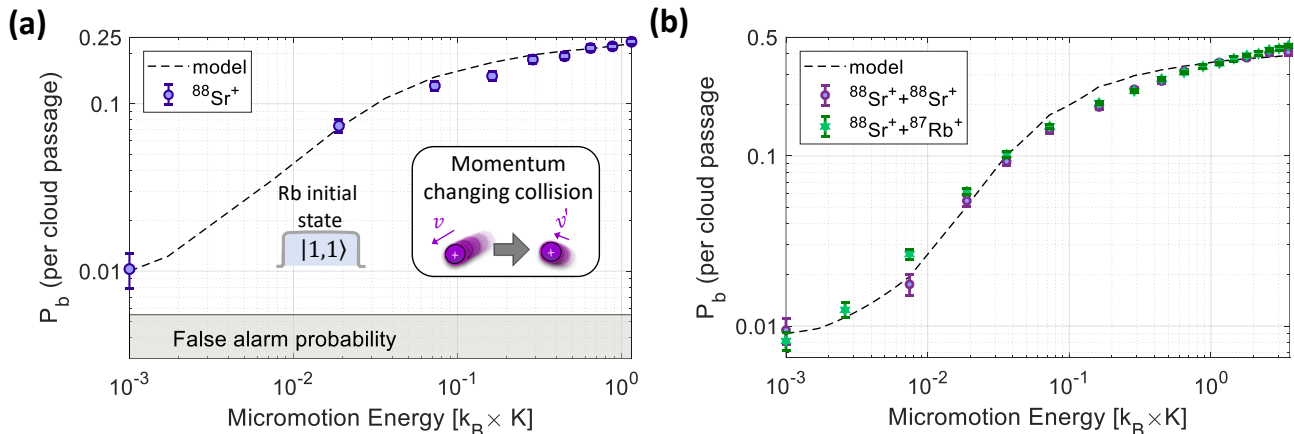


Figure 4. **Momentum changing collisions** can convert micromotion energy of an ion into secular motion, and be detected with probability  $P_b$  per passage of the cloud. (a) Single ion crystal of  $^{88}\text{Sr}^+$ . (b) Two ion crystals of  $^{88}\text{Sr}^+ - ^{88}\text{Sr}^+$  (purple) and  $^{88}\text{Sr}^+ - ^{87}\text{Rb}^+$  (green). Dashed lines correspond to numerically simulated values which reveal an average Langevin rate of  $\kappa_L = 0.29 \pm 0.02$  per passage of the cloud. Bars represent  $1\sigma$  binomial uncertainties.

the Langevin probability using the ions, based on momentum-changing collisions [56, 57] which are elastic scattering events whose scattering angle is not near zero [58] as schematically shown in Fig. 1b. These collisions lead to redistribution of the kinetic energy of the colliding bodies that is approximately isotropic, and are usually considered in the context of buffer-gas cooling [56, 59] or ions mobility [49]. Momentum-changing collisions are correlated with Langevin collisions, and their rate coefficient is almost identical to the Langevin collision rate coefficient [56, 59]. Therefore, measurement of momentum-changing collisions allows for direct estimation of the Langevin probability.

### III. EXPERIMENTAL STUDY

#### A. Apparatus

We study the interaction between neutral  $^{87}\text{Rb}$  atoms and  $^{87}\text{Rb}^+$ . Two vacuum chambers positioned 25 cm apart are used to trap and laser-cool a cloud of  $^{87}\text{Rb}$  atoms at a few  $\mu\text{K}$  (right chamber), and short chains of ions cooled near their ground-state in a Paul trap (left chamber) as shown in Fig. 2. The neutral cloud is initially trapped into a magneto-optical trap and subsequently loaded into an off-resonant optical lattice, where the spin state  $|F, M\rangle$  of the Rb atoms is determined using optical pumping and microwave pulses.

Owing to the closed electronic shell structure of  $^{87}\text{Rb}^+$ , it lacks the necessary optical transitions which could enable its direct cooling and detection. Instead, we load and trap a two ions crystal that is composed of one  $^{88}\text{Sr}^+$  and one  $^{87}\text{Rb}^+$  via subsequent photo-ionization of a neutral Sr and neutral  $^{87}\text{Rb}$  gas. We

use the  $^{88}\text{Sr}^+$  ion to laser-cool and sympathetically cool all motional modes of the crystal near the ground-state, to compensate for excess micro-motion, to enable logic detection of exothermic processes of  $^{87}\text{Rb}^+$  and for calibration of the Langevin collision rate. We routinely verify the masses of the two ions via mass spectrometry. Further details on our experimental apparatus can be found in Refs. [47, 60, 61].

The experiment follows the sequence presented in Fig. 2. We shuttle the neutral cloud towards the Paul trap by varying the relative optical frequencies of two counter-propagating optical lattice beams. This allows for interaction between an ion and on average one atom during the passage of the sparse atomic cloud through the Paul trap.

#### B. Logic detection of hyperfine changing collisions

We measure the hyperfine changing probability per passage of the atomic cloud using the quantum-logic technique developed in Ref. [47]. We initialize the  $^{88}\text{Sr}^+$  spin upwards, and prepare the  $^{87}\text{Rb}$  spins at each of the five  $|F = 2, M\rangle$  states (integer  $|M| \leq 2$ ) in a randomized manner and assume that the spin of  $^{87}\text{Rb}^+$  is in a complete mixed state. We measure the collision-induced heating of the crystal via carrier shelving thermometry; This technique maps hot (cold) motional states of the crystal into a bright (dark) state of the logic ion, that is subsequently detected via state-dependent fluorescence. We use the same experimental parameters as in Ref. [47], which feature high sensitivity to energy release of the hyperfine energy  $E_{\text{hpf}}$  at hundreds of  $k_B \times \text{mK}$ , but reduced sensitivity to trap-induced heating at about  $\lesssim 1 k_B \times \text{mK}$ .

In Fig. 3a we plot the probability that the logic ion

in a  $^{88}\text{Sr}^+ - ^{87}\text{Rb}^+$  crystal is bright (hot) after one passage of the cloud (grey). Here, heating associated with release of hyperfine energy by a neutral  $^{87}\text{Rb}$  atom is associated with either a collisional process with the logic  $^{88}\text{Sr}^+$  ion (mainly via spin-exchange) or with a collision with the  $^{87}\text{Rb}^+$  ion (via charge-exchange). To measure the statistics of these two processes, we additionally measure the hyperfine release probability for a different configuration, a crystal of two  $^{88}\text{Sr}^+$  ions. In Fig. 3a we present the total probability that at least one of these ions is bright (purple bars). Using the logic procedure detailed in Methods, we can discern between the hyperfine changing probability per passage of the neutral cloud  $\bar{P}_{\text{hpf}}$  with the  $^{88}\text{Sr}^+$  ion or with the  $^{87}\text{Rb}^+$  ion, as shown in Fig. 3b. Evidently, the hyperfine-changing collision probability between a single pair of  $^{87}\text{Rb}^+ - ^{87}\text{Rb}$  (green bar) is almost an order of magnitude smaller than the hyperfine-changing probability between a single pair of  $^{88}\text{Sr}^+ - ^{87}\text{Rb}$  (purple bar).

### C. Langevin probability estimation

We developed a technique that enables estimation of the Langevin probability per passage of the cloud via measurement of momentum changing collisions. We apply a constant electric field  $E_{\text{dc}}$  which pushes the ions from the RF-null line, and by that increases their excess micro-motion along the RF field lines, as shown schematically in Fig. 2. Owing to the high micro-motion frequency compared to the trap secular frequencies, and to the micro-motion axis being perpendicular to both the cooling and shelving light, the secular motion is efficiently cooled even at large micro-motion amplitudes.

A momentum changing collision with a neutral atom redistributes the ion's micro-motion energy and heats the secular modes of motion [48]. Carrier-shelving thermometry, which is mostly sensitive to the ion's secular motion, can then detect this heating.

We apply this technique and measure the probability of hot events  $P_b$  (ion appears bright after two shelving attempts) per passage of the cloud as a function of the micromotion energy (see Methods for details). The neutral atoms are prepared in their lowest ground state  $|1, 1\rangle_{\text{Rb}}$  to suppress heating via release of internal energy. In Fig. 4a we present this probability for a one ion crystal of  $^{88}\text{Sr}^+$ . Gray-shaded area indicate our false-alarm probability (0.5%) measured in the absence of the atomic cloud. We repeat the experiment for two additional configurations, a  $^{88}\text{Sr}^+ - ^{88}\text{Sr}^+$  crystal and a  $^{88}\text{Sr}^+ - ^{87}\text{Rb}^+$  crystal as shown in Fig. 4b. Evidently, the greater the micromotion energy, the more efficiently momentum-changing collisions are observed.

We numerically simulated the dynamics of a trapped ions crystals with excess micromotion following Poissonian-distributed collisions, and calculated the

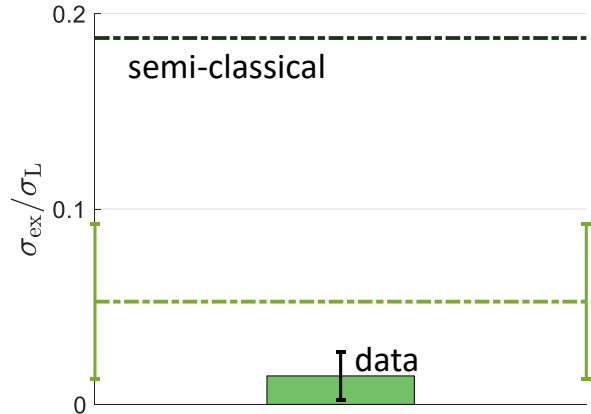


Figure 5. **Quantum Suppression of charge exchange.** The probability for hyperfine de-excitation during a resonant charge-exchange reaction (green bar) is 12-fold suppressed with respect to the semiclassical value  $\sigma_{\text{ex}} = 3\sigma_{\text{L}}/16$  (see text). Dash green line is an upper bound on the measured value if the effect of the trap on the dynamics is uncorrected. Bars represent  $1\sigma$  binomial uncertainties.

shelving probability as detailed in Methods. We obtain the numerically-calculated black curves using only two free parameters: the ion's effective temperature  $T$  at the onset of a collision, and the average number of collisions  $\kappa_{\text{L}}$  per passage of the cloud per ion. The former (latter) predominantly determines the shelving probability at very low (high) micromotion energies. We obtain good agreement with the theoretical model for  $T = 0.6 \pm 0.1$  mK and  $\kappa_{\text{L}} = 0.29 \pm 0.02$ . We also find from Fig. 4b that  $\kappa_{\text{L}}^{\text{Rb}^+}/\kappa_{\text{L}}^{\text{Sr}^+} = 0.97 \pm 0.06$  which is in excellent agreement with the theoretical value near 1.

### D. Absolute rate estimation

Using the rate of Langevin collisions per passage of the cloud  $\kappa_{\text{L}}$  and the data in Fig. 3, we can directly estimate the probability of a hyperfine-change via charge exchange reaction (per one Langevin collision),  $p_{\text{ex,L}} = (0.053 \pm 0.04)$  which is approximately  $p_{\text{ex,L}} \approx \bar{P}_{\text{hpf}}/\kappa_{\text{L}}$  (see Methods).

Owing to the presence of the ion trap, binary collisions of the atom-ion pair can efficiently form weakly bound states with the trap assistance [62]. At cold temperatures, the bound-states enhance the measured inelastic rate by increasing the number of events for which the pair interacts at short-range. We follow the methodology in [62] and show that the charge exchange rate corrected for the formation of bound-states is  $\sigma_{\text{ex}} = (0.015 \pm 0.012)\sigma_{\text{L}}$  which is greatly suppressed compared with the semi-classical value of  $3\sigma_{\text{L}}/16$  (for

$\xi = 3/8$ ), as shown in Fig. 5. Notably, the bound-state formation can only enhance the measured rate and cannot reverse a reaction, because the hyperfine-energy release of a charge exchange collision efficiently breaks the weakly-bound molecule. The probability  $p_{\text{ex,L}}$ , which is uncorrected for the bound-state formation, therefore casts an upper bound on the measured charge-exchange rate, as shown in dashed green line. Evidently, even this upper-bound is well suppressed with respect to the semi-classical value.

#### IV. DISCUSSION AND OUTLOOK

In this work, we analyzed resonant charge-exchange collisions between atom and ion pairs of  $^{87}\text{Rb} - ^{87}\text{Rb}^+$  by monitoring exothermic spin change via a  $^{88}\text{Sr}^+$  logic ion. We probed momentum changing collisions to estimate for the Langevin collision rate in our setup and to obtain an absolute scale for the resonant charge exchange rate. Our results show significant suppression of charge-exchange reactions for channels that change their hyperfine state with respect to the semi-classically predicted value.

The suppressed measured value of resonant charge-exchange likely originates from suppression at the ultracold  $s$ -wave regime (below  $79 k_B \times \text{nK}$ ), which is conjectured to persist at our higher experimental energies (hundreds of  $k_B \times \mu\text{K}$  from the fits in Fig. 4a-b) via the partial-wave phase-locking mechanism [20, 21]. Remarkably, the long range of the polarization-potential interaction which sets the  $s$ -wave limit to a very low temperature, also rendered the quantum nature of the reaction robust to the presence of many partial waves. It is expected that multi-channel quantum scattering analysis can utilize our results to calibrate for the differential scattering shift of the molecular potentials and to extend the study of the phase-locking mechanism. Application of the two techniques used in this work, namely accurate calibration for Langevin collisions rate and quantum logic technique for measurement of inelastic cross-sections, can potentially extend the range of processes and hybrid atom-ion systems that can be studied experimentally.

While the exchange between  $^{87}\text{Rb} - ^{87}\text{Rb}^+$  is suppressed in the cold regime, other isotopes or pairs of alkali ions and their parent neutral atoms would exhibit different cross-sections [20]; owing to the sinusoidal dependence of the cross-section on the phase shift in Eq. (1), it is expected that most atoms would deviate from the semi-classical value if the differential phase shift of different atoms is uniformly sampled, thus featuring suppression or enhancement [20]. An enhanced coupling can potentially allow for efficient preparation and detection of the nuclear spin state of cold alkali ions, which is otherwise inaccessible owing to its great isola-

tion from the environment. Intriguingly, this isolation, which originates from the closed electronic shells and the small gyromagnetic ratio, is expected to grant long spin-coherence times which could potentially be used in metrology or quantum information applications [63–65].

#### ACKNOWLEDGMENTS

This work was supported by the Israeli Science Foundation and the Goldring Family Foundation. We thank Marko Cetina, Maks Walewski, Mathew Frye and Michał Tomza for fruitful discussions.

# Methods

## HYPERFINE CHANGE DURING CHARGE EXCHANGE

In this section we estimate the probability for a hyperfine change during a charge exchange collision within the Degenerate-Internal-State Approximation (DISA). The scattering we consider here involves three different sets of spin operators  $\mathbf{S}$  for the electron,  $\mathbf{I}_1$  for the nucleus associated with the neutral atom pre-collision and  $\mathbf{I}_2$  for the nucleus associated with the ion pre-collision. Within the DISA formalism, the initial and final states we consider are given in terms of the hyperfine state of the neutral atom (and spin state of the ion) whereas the transition between them is manifested by the exchange operator.

The charge exchange operator is given by [53]

$$\Pi_{\text{ex}} = \mathbb{1}_S \otimes (P_g - P_u), \quad (2)$$

where  $\mathbb{1}_S$  is the electron spin identity matrix and

$$P_g = \sum_{I \text{ odd}} \sum_{I_z = -I}^I |I, I_z\rangle \langle I, I_z|, \quad (3)$$

is the projection operator over the *gerade* subspace, casted with the quantum numbers of the total nuclear spin ( $\mathbf{I} = \mathbf{I}_1 + \mathbf{I}_2$ ) where  $I$  is the total nuclear spin number of the complex and  $I_z$  is the projection along the quantization axis. The projection over the *ungerade* subspace is  $P_u = \mathbb{1}_{I_1} \otimes \mathbb{1}_{I_2} - P_g$  where  $\mathbb{1}_{I_1}, \mathbb{1}_{I_2}$  are the identity operators of the two nuclear spins.

In terms of the uncoupled basis  $|I_{1z}, I_{2z}\rangle$  (where  $I_{1z}, I_{2z}$  are the quantum numbers for the projection along the quantization axis of the operators  $\mathbf{I}_1, \mathbf{I}_2$  respectively) the matrix elements of the charge exchange operator take a simple form

$$\langle I_{1z}, I_{2z} | \Pi_{\text{ex}} | I'_{1z}, I'_{2z} \rangle = \delta_{I_{1z}, I'_{1z}} \delta_{I_{2z}, I'_{2z}}, \quad (4)$$

where  $\delta$  is the kronecker delta function.

To consider hyperfine changing collisions we cast the two projection operators by

$$P_F = \left( \sum_{M=-F}^F |F, M\rangle \langle F, M| \right) \otimes \mathbb{1}_{I_2} \quad (5)$$

where  $F, M$  are the quantum numbers associated with the total spin operator  $\mathbf{F} = \mathbf{S} + \mathbf{I}_1$  of the neutral atom, which can be represented in the uncoupled basis  $|S_z, I_{1z}\rangle$  via the Clebsch-Gordan transformation.

Here we consider a  $^{87}\text{Rb} - ^{87}\text{Rb}^+$  pair with  $S = 1/2$ ,  $I_1 = I_2 = 3/2$ . We consider the neutral  $^{87}\text{Rb}$  atom in a statistical mixture in the upper hyperfine manifold

$$\rho_1 = \frac{1}{5} \sum_{M=-2}^2 |F=2, M\rangle \langle F=2, M|, \quad (6)$$

and the nuclear spin of the ion in a completely mixed state

$$\rho_2 = \frac{1}{4} \sum_{m=-3/2}^{3/2} |m\rangle \langle m|, \quad (7)$$

composing the total spin density-matrix  $\rho_{\text{tot}} = \rho_1 \otimes \rho_2$ .

We can estimate the spin parameter  $\xi$  using the semi-classical Degenerate-Internal State Approximation [66–69], which gives the transition probability from an initial state to a final state by the exchange operator  $\Pi_{\text{ex}}$ . For our configuration this operator is given by

$$\xi = \text{Tr}(P_1 \Pi_{\text{ex}} \rho_{\text{tot}} \Pi_{\text{ex}} P_1) = \frac{3}{8}, \quad (8)$$

where the projection operator  $P_1$  constraints the final state to be in the lower hyperfine manifold ( $F = 1$ ), to account for the experimental configuration in which the Rb atom changes its hyperfine by the collision.

This formalism allows also estimation of the parameter  $\xi$  in other configurations. For example, if we consider the transition to all output channels possible then  $\xi = \text{Tr}(\Pi_{\text{ex}} \rho_{\text{tot}} \Pi_{\text{ex}}) = 1$ , owing to the unitarity of the scattering process. Alternatively, if we consider the special case of atoms with no nuclear spin then  $P_g = 0$  and  $P_u = \mathbb{1}_S \otimes \mathbb{1}_{I_1} \otimes \mathbb{1}_{I_2}$  then again  $\xi = 1$  for any initial density matrix.

## LOGIC DETECTION OF CHARGE EXCHANGE PROBABILITY

In this section, we present the logic analysis that allows to associate the hyperfine-changing collision probability to each of the processes, following the technique in Ref. [47].

We performed electron-shelving detection of  $^{88}\text{Sr}^+$  and recorded the probability  $\tilde{P}_b(F, M)$  that at least one  $^{88}\text{Sr}^+$  ion appears bright after passage of the Rb cloud (prepared in a spin state  $|F, M\rangle_{\text{Rb}}$ ). Additional processes that are associated with technical errors as well as trap induced heating could lead to a nonzero false alarm probability that is superposed on the probability of hyperfine changing collisions. We quantified this false-alarm probability by measuring the scattering of the two channels  $|1, \pm 1\rangle_{\text{Rb}}$  in which hyperfine-changing collisions are suppressed due to energy conservation for compensated micro-motion. We can then statistically correct for this false-alarm by construction of the probability  $P_b(M)$

$$P_b(M) = \tilde{P}_b(2, M) - \frac{1}{2}(\tilde{P}_b(1, 1) + \tilde{P}_b(1, -1)) \quad (9)$$

as shown in Fig. 3a for the two configurations. Notably, our false-alarm probability is small and almost constant

per  $^{88}\text{Sr}^+$ :  $\bar{P}_b(1, 1) = \bar{P}_b(1, -1) = 0.016 \pm 0.002$  for the  $^{88}\text{Sr}^+ - ^{87}\text{Rb}^+$  crystal and is almost doubled  $\bar{P}_b(1, 1) = 0.041 \pm 0.004$  and  $\bar{P}_b(1, -1) = 0.035 \pm 0.004$  for the  $^{88}\text{Sr}^+ - ^{88}\text{Sr}^+$  configuration, owing to having a pair of  $^{88}\text{Sr}^+$  ions.

Taking into account our finite detection efficiency  $\eta = 0.8$  for this trapping configuration [47], we can find the average probability of hyperfine-changing collision per passage of the cloud per one Sr ion by

$$\bar{P}_{\text{hpf}}^{(\text{Sr})} = \frac{1}{10\eta} \sum_{M=-2}^2 P_b^{(\text{Sr}-\text{Sr})}(M), \quad (10)$$

where  $P_b^{(\text{Sr}-\text{Sr})}(M)$  is the probability in Eq. (9) for the configuration of two-Strontium ion crystal. The hyperfine changing probability for a single Rb ion is then given by

$$\bar{P}_{\text{hpf}}^{(\text{Rb})} = \frac{1}{5\eta} \left( \sum_{M=-2}^2 P_b^{(\text{Rb}-\text{Sr})}(M) \right) - \bar{P}_{\text{hpf}}^{(\text{Sr})}, \quad (11)$$

which are presented in Fig. 3b.

## MICROMOTION DYNAMICS

In this section, we define the micromotion energy and describe its experimental calibration. The average position of a trapped ion is determined by the Mathieu equation. In the presence of time-independent electric field  $\mathbf{E}_{\text{DC}}$  its solution is given by [70]

$$R_i(t) = (x_i + A_i \cos(\omega_i t + \phi_i)) \left( 1 + \frac{q_i}{2} \cos(\Omega t) \right) \quad (12)$$

where  $\omega_i$  is the secular trap frequency for each axis  $i \in x, y, z$ ,  $\Omega$  is the fast micromotion frequency,  $A_i$  is the secular motion amplitude of the ion,  $\phi_i$  is a random phase and  $q_i$  is the trap parameter determining the inherent micromotion amplitude for that axis. For sufficiently weak DC fields as we consider here, the offset from the RF null is given by

$$x_i = \frac{eE_{\text{DC},i}}{m_{\text{ion}}\omega_i^2}, \quad (13)$$

where  $e$  is the electron charge and  $m_{\text{ion}}$  is the ion's mass. According to Eq. (12), the offset generates time-dependent oscillations whose time-averaged kinetic energy is

$$E_{\text{EMM}} = \sum_i \frac{m_{\text{ion}}\Omega^2 q_i^2 x_i^2}{16}. \quad (14)$$

We experimentally control for  $x_i$ , by setting the voltage  $V$  on one of the electrodes in the trap. We calibrated the linear dependence of  $x_i(V)$  via imaging of the ion

position at different voltages. In our segmented blade trap  $q_y = -q_x \approx 0.14$  while  $q_z$  is negligible.  $\Omega = 26.5$  MHz while  $0.45 \text{ MHz} \leq \omega_i \leq 1.5 \text{ MHz}$  and the electric field axis is along  $(\hat{x} + \hat{y})\sqrt{2}$ .

## NUMERICAL SIMULATIONS

In this section, we detail the numerical simulations which allow inference of the Langevin rate from the data in Fig. 4. We describe the position of the ions using the formalism in Ref. [70] which describes both the secular motion by the trapping and Coulomb forces as well as fast dynamics associated with inherent and excess micro-motion induced by stray fields. The initial energy of the ion is randomly generated from the probability distribution function [71]

$$f(E) = \frac{E^2}{2k_{\text{B}}^3 T^3} \exp\left(-\frac{E}{k_{\text{B}}T}\right). \quad (15)$$

with initial temperature  $T$ .

We assume that in a given passage of a cloud each ion in the chain can experience Langevin collisions, whose occurrence follows Poissonian statistics with an average rate of  $\kappa_{\text{L}}$  that is assumed to be independent of the collision energy. We consider a Langevin type collision as an instantaneous elastic event in a random time where the ion's position is maintained but its instantaneous velocity  $\mathbf{v}_i$  is updated to [47, 48]

$$\mathbf{v}_i \rightarrow (1 - r + r\mathcal{R}(\varphi_{\text{L}}))(\mathbf{v}_i - \mathbf{v}_{\text{a}}) + \mathbf{v}_{\text{a}}, \quad (16)$$

where  $\mathbf{v}_{\text{a}}$  is the atom velocity which is randomly drawn from a Maxwell-Boltzman distribution with temperature of  $10 \mu\text{K}$ . The masses ratio  $r = \mu/m_i \approx 0.5$  where  $\mu = m_i m_{\text{a}} / (m_i + m_{\text{a}})$  is the reduced mass, and  $\mathcal{R}$  is the rotation matrix in the collision plane with scattering angle  $\phi_{\text{L}}$  that is randomly generated. We calculated the distribution probability function  $f(\phi_{\text{L}})$  independently by classical scattering dynamics [59], and found that for spiraling collisions it is approximately given by  $f(\phi_{\text{L}}) = 0.384 - 0.013\phi_{\text{L}} - 0.014\phi_{\text{L}}^2$  for  $0 \leq \phi_{\text{L}} \leq \pi$ .

The instantaneous change of velocity by collisions leads to distribution of the ion's micro-motion energy to all direction and to the secular motion. Denoting by  $A_i$  the amplitudes of the secular motion of the Sr ion after the passage of the cloud, we calculate the detection probability of a hot Sr ion by

$$P_b = \cos^2 \left( \frac{\pi}{2} \prod_i J_0(k_i A_i) \right), \quad (17)$$

assuming a long detection pulse compared to the motional cycle. Here  $k_i$  denote the components of the shelving beam wavenumber, along the modes axes and  $J_0$  is the zeroth order Bessel function. Notably, the sensitivity of our experimental (and numerical) technique is

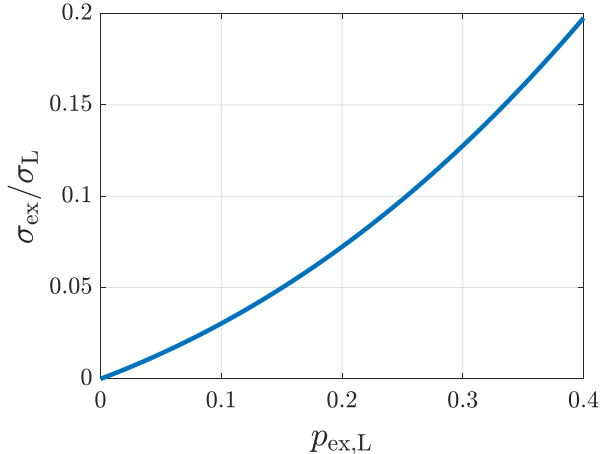


Figure 6. **Charge Exchange probability in the presence of the trap.** Numerical calculation of the measured hyperfine-changing charge exchange collisions per Langevin collision  $p_{\text{ex,L}}$  in the presence of the ion trap with respect to the free space value  $\sigma_{\text{ex}}/\sigma_{\text{L}}$ . The enhancement of the measured charge-exchange reaction originates from trap-assisted molecules that increase the interaction times at short ranges

limited to detection of secular motion along the shelving beam axis.

We repeat the simulation about  $5 \times 10^4$  times and average the results for each value of  $T$  and  $\kappa_{\text{L}}$  we consider. We find a good correspondence with the measured data for  $T = 0.6 \pm 0.1$  mK and for  $\kappa_{\text{L}} = 0.29 \pm 0.02$ .

## TRAP-ASSISTED BOUND STATES

Owing to the breaking of translation-invariance symmetry in the presence of the ion trap, short-lived bound states can form in binary collisions of atom-ion pairs. In such a bound state, a single atom-ion pair can spiral and get into close contact  $n \geq 1$  times which could enhance the measured inelastic rate over the charge exchange rate in free space. We simulate the effect of bound states using a numerical molecular dynamics simulation similar to Refs. [17, 18, 71] and construct the probability mass function of  $n$ ,  $\text{PMF}(n)$  from  $\sim 2500$  Langevin collisions for our experimental parameters.

Owing to the release of hyperfine energy in the considered charge-exchange collision, we can relate the free space exchange probability  $\sigma_{\text{ex}}/\sigma_{\text{L}}$  to effective measured probability in the presence of the trap by

$$p_{\text{ex,L}} = \sum_n \text{PMF}(n) \left(1 - \frac{\sigma_{\text{ex}}}{\sigma_{\text{L}}}\right)^{n-1} \left(\frac{\sigma_{\text{ex}}}{\sigma_{\text{L}}}\right), \quad (18)$$

as shown in Fig. 6.

Independent of the bound state analysis, the experimental value  $p_{\text{ex,L}}$  can be related to the charge-exchange probability per passage of the cloud  $\bar{P}_{\text{hpf}}$  by taking into account the Poissonian distribution of collision events of the trapped ions with different atoms at finite values of  $\kappa_{\text{L}}$ . For small rates we can approximate this relation by accounting for one or two collisions events through

$$\bar{P}_{\text{hpf}} = \kappa_{\text{L}} e^{-\kappa_{\text{L}}} \left( p_{\text{ex,L}} + \frac{\kappa_{\text{L}}}{2} (2p_{\text{ex,L}} - p_{\text{ex,L}}^2) \right). \quad (19)$$

- 
- [1] P. Paliwal, N. Deb, D. M. Reich, A. v. d. Avoird, C. P. Koch, and E. Narevicius, *Nature Chemistry* **13**, 94 (2021).
  - [2] T. Köhler, K. Góral, and P. S. Julienne, *Reviews of modern physics* **78**, 1311 (2006).
  - [3] C. Chin, R. Grimm, P. Julienne, and E. Tiesinga, *Reviews of Modern Physics* **82**, 1225 (2010).
  - [4] I. Bloch, J. Dalibard, and S. Nascimbene, *Nature Physics* **8**, 267 (2012).
  - [5] F. Schäfer, T. Fukuhara, S. Sugawa, Y. Takasu, and Y. Takahashi, *Nature Reviews Physics* **2**, 411 (2020).
  - [6] K. Jachymski and A. Negretti, *Physical Review Research* **2**, 033326 (2020).
  - [7] C. Gross, T. Zibold, E. Nicklas, J. Esteve, and M. K. Oberthaler, *Nature* **464**, 1165 (2010).
  - [8] M. Safronova, D. Budker, D. DeMille, D. F. J. Kimball, A. Derevianko, and C. W. Clark, *Reviews of Modern Physics* **90**, 025008 (2018).
  - [9] K. M. Jones, E. Tiesinga, P. D. Lett, and P. S. Julienne, *Reviews of Modern Physics* **78**, 483 (2006).
  - [10] S. Ospelkaus, K.-K. Ni, D. Wang, M. De Miranda, B. Neyenhuis, G. Quéméner, P. Julienne, J. Bohn, D. Jin, and J. Ye, *Science* **327**, 853 (2010).
  - [11] Y. Liu, M.-G. Hu, M. A. Nichols, D. Yang, D. Xie, H. Guo, and K.-K. Ni, *Nature* **593**, 379 (2021).
  - [12] F. Schmidt, D. Mayer, Q. Bouton, D. Adam, T. Lausch, J. Nettersheim, E. Tiemann, and A. Widera, *Physical Review Letters* **122**, 013401 (2019).
  - [13] P. Weckesser, F. Thielemann, D. Wiater, A. Wojciechowska, L. Karpa, K. Jachymski, M. Tomza, T. Walker, and T. Schaetz, *Nature* **600**, 429 (2021).
  - [14] T. Feldker, H. Füst, H. Hirzler, N. Ewald, M. Mazzanti, D. Wiater, M. Tomza, and R. Gerritsma, *Nature Physics* **16**, 413 (2020).
  - [15] K. Jachymski, M. Krych, P. S. Julienne, and Z. Idziaszek, *Physical Review A* **90**, 042705 (2014).
  - [16] M. Tomza, K. Jachymski, R. Gerritsma, A. Negretti, T. Calarco, Z. Idziaszek, and P. S. Julienne, *Reviews of modern physics* **91**, 035001 (2019).
  - [17] M. Cetina, A. T. Grier, and V. Vuletić, *Physical review letters* **109**, 253201 (2012).
  - [18] M. Pinkas, Z. Meir, T. Sikorsky, R. Ben-Shlomi, N. Akerman, and R. Ozeri, *New Journal of Physics* **22**, 013047 (2020).

- [19] R. S. Lous and R. Gerritsma, arXiv preprint arXiv:2206.14471 (2022).
- [20] R. Côté and I. Simbotin, *Physical Review Letters* **121**, 173401 (2018).
- [21] T. Sikorsky, M. Morita, Z. Meir, A. A. Buchachenko, R. Ben-Shlomi, N. Akerman, E. Narevicius, T. V. Tscherbul, and R. Ozeri, *Physical review letters* **121**, 173402 (2018).
- [22] A. T. Grier, M. Cetina, F. Oručević, and V. Vuletić, *Physical review letters* **102**, 223201 (2009).
- [23] J. Schmidt, P. Weckesser, F. Thielemann, T. Schaetz, and L. Karpa, *Physical review letters* **124**, 053402 (2020).
- [24] L. Ratschbacher, C. Zipkes, C. Sias, and M. Köhl, *Nature Physics* **8**, 649 (2012).
- [25] A. Härter and J. Hecker Denschlag, *Contemporary Physics* **55**, 33 (2014).
- [26] F. H. Hall, M. Aymar, N. Bouloufa-Maafa, O. Dulieu, and S. Willitsch, *Physical review letters* **107**, 243202 (2011).
- [27] T. Sikorsky, Z. Meir, R. Ben-Shlomi, N. Akerman, and R. Ozeri, *Nature communications* **9**, 1 (2018).
- [28] A. Mohammadi, A. Krüchow, A. Mahdian, M. Deiß, J. Pérez-Ríos, H. da Silva Jr, M. Raoult, O. Dulieu, and J. H. Denschlag, *Physical Review Research* **3**, 013196 (2021).
- [29] W. G. Rellergert, S. T. Sullivan, S. Kotochigova, A. Petrov, K. Chen, S. J. Schowalter, and E. R. Hudson, *Physical review letters* **107**, 243201 (2011).
- [30] T. V. Tscherbul, P. Brumer, and A. A. Buchachenko, *Physical Review Letters* **117**, 143201 (2016).
- [31] R. Saito, S. Haze, M. Sasakawa, R. Nakai, M. Raoult, H. Da Silva Jr, O. Dulieu, and T. Mukaiyama, *Physical Review A* **95**, 032709 (2017).
- [32] A. Krüchow, A. Mohammadi, A. Härter, J. H. Denschlag, J. Pérez-Ríos, and C. H. Greene, *Physical Review Letters* **116**, 193201 (2016).
- [33] H. Hirzler, R. Lous, E. Trimby, J. Pérez-Ríos, A. Safavi-Naini, and R. Gerritsma, *Physical Review Letters* **128**, 103401 (2022).
- [34] F. H. Hall and S. Willitsch, *Physical review letters* **109**, 233202 (2012).
- [35] M. Tomza and M. Lisaj, *Physical Review A* **101**, 012705 (2020).
- [36] H. Li, S. Jyothi, M. Li, J. Kłos, A. Petrov, K. R. Brown, and S. Kotochigova, *Physical Chemistry Chemical Physics* **22**, 10870 (2020).
- [37] N. Ewald, T. Feldker, H. Hirzler, H. Fürst, and R. Gerritsma, *Physical Review Letters* **122**, 253401 (2019).
- [38] S. Haze, R. Saito, M. Fujinaga, and T. Mukaiyama, *Physical Review A* **91**, 032709 (2015).
- [39] S. Schmid, A. Härter, and J. H. Denschlag, *Physical review letters* **105**, 133202 (2010).
- [40] P. F. Staunum, K. Højbjerg, R. Wester, and M. Drewsen, *Physical review letters* **100**, 243003 (2008).
- [41] I. Sivarajah, D. Goodman, J. Wells, F. Narducci, and W. Smith, *Physical Review A* **86**, 063419 (2012).
- [42] K. S. Kleinbach, F. Engel, T. Dieterle, R. Löw, T. Pfau, and F. Meinert, *Physical review letters* **120**, 193401 (2018).
- [43] R. Ben-shlomi, R. Vexiau, Z. Meir, T. Sikorsky, N. Akerman, M. Pinkas, O. Dulieu, and R. Ozeri, *Physical Review A* **102**, 031301(R) (2020).
- [44] K. Ravi, S. Lee, A. Sharma, G. Werth, and S. Rangwala, *Nature Communications* **3**, 1 (2012).
- [45] S. Dutta and S. Rangwala, *Physical Review A* **97**, 041401 (2018).
- [46] A. Mahdian, A. Krüchow, and J. H. Denschlag, *New Journal of Physics* **23**, 065008 (2021).
- [47] O. Katz, M. Pinkas, N. Akerman, and R. Ozeri, *Nature Physics* **18**, 533 (2022).
- [48] C. Zipkes, L. Ratschbacher, C. Sias, and M. Köhl, *New Journal of Physics* **13**, 053020 (2011).
- [49] R. Côté and A. Dalgarno, *Physical Review A* **62**, 012709 (2000).
- [50] R. Côté, in *Advances in atomic, molecular, and optical physics*, Vol. 65 (Elsevier, 2016) pp. 67–126.
- [51] R. D. Levine, *Molecular reaction dynamics* (Cambridge University Press, 2009).
- [52] J. K. Mitchell and E. N. Fortson, *Physical Review A* **8**, 704 (1973).
- [53] S. S. Townsend, *Charge Exchange Optical Pumping.*, Ph.D. thesis, University of New Hampshire (1977).
- [54] Charge exchange collisions are characterized by inversion of the scattering amplitude  $f(\pi - \theta)$  where  $f(\theta)$  is the scattering amplitude of the elastic collision with scattering angle  $\theta$ . At higher energies, the exchange is associated with glancing collisions whose scattering is peaked at  $\theta = 0$ , and therefore charge exchange is associated with scattering that is peaked at  $f(\pi)$ . In the cold regime however, charge exchange is associated with Langevin collisions, the scattering amplitude  $f(\theta)$  of which is approximately uniform in  $\theta$ , hindering the distinction of  $f(\pi - \theta)$  and  $f(\theta)$ .
- [55] J. R. Zimmerman and D. Williams, *Physical Review* **76**, 350 (1949).
- [56] K. Chen, S. T. Sullivan, and E. R. Hudson, *Physical review letters* **112**, 143009 (2014).
- [57] Z. Meir, M. Pinkas, T. Sikorsky, R. Ben-shlomi, N. Akerman, and R. Ozeri, *Physical Review Letters* **121**, 053402 (2018).
- [58] We adopt the definitions in Ref. [56] which distinguishes momentum-changing collisions from elastic glancing collisions. The latter are predominantly forward-scattering events and barely redistribute the kinetic energy (c.f. [57, 72]).
- [59] M. Cetina *et al.*, *Hybrid approaches to quantum information using ions, atoms and photons*, Ph.D. thesis, Massachusetts Institute of Technology (2011).
- [60] Z. Meir, T. Sikorsky, R. Ben-shlomi, N. Akerman, M. Pinkas, Y. Dallal, and R. Ozeri, *Journal of Modern Optics* **65**, 501 (2018).
- [61] R. Ben-shlomi, M. Pinkas, Z. Meir, T. Sikorsky, O. Katz, N. Akerman, and R. Ozeri, *Physical Review A* **103**, 032805 (2021).
- [62] M. Pinkas, O. Katz, J. Wengrowicz, N. Akerman, and R. Ozeri, arXiv preprint arXiv:2208.06904 (2022).
- [63] P. Wang, C.-Y. Luan, M. Qiao, M. Um, J. Zhang, Y. Wang, X. Yuan, M. Gu, J. Zhang, and K. Kim, *Nature communications* **12**, 1 (2021).
- [64] R. Shaham, O. Katz, and O. Firstenberg, *Nature Physics* **18**, 506 (2022).
- [65] O. Katz, R. Shaham, and O. Firstenberg, *Science advances* **7**, eabe9164 (2021).

- [66] A. Maan, E. Tiesinga, H. Stoof, and B. Verhaar, *Physica B: Condensed Matter* **165**, 17 (1990).
- [67] B. Verhaar, J. Koelman, H. Stoof, O. Luiten, and S. Crampton, *Physical Review A* **35**, 3825 (1987).
- [68] A. Dalgarno, *Proceedings of the Royal Society of London. Series A. Mathematical and Physical Sciences* **262**, 132 (1961).
- [69] A. Dalgarno and M. Rudge, *Proceedings of the Royal Society of London. Series A. Mathematical and Physical Sciences* **286**, 519 (1965).
- [70] A. Bermudez, P. Schindler, T. Monz, R. Blatt, and M. Müller, *New Journal of Physics* **19**, 113038 (2017).
- [71] Z. Meir, *Dynamics of a single, ground-state cooled and trapped ion colliding with ultracold atoms: a micromotion tale*, Ph.D. thesis, The Weizmann Institute of Science (Israel) (2017).
- [72] C. Zipkes, S. Palzer, L. Ratschbacher, C. Sias, and M. Köhl, *Physical review letters* **105**, 133201 (2010).